DIFFERENTIAL PHASE CONTRAST CT – CHARACTERICS OF SIGNAL AND NOISE

Xiangyang Tang, Yi Yang and Shaojie Tang

Department of Radiology and Imaging Sciences, Emory University School of Medicine
Atlanta, Georgia 30097, USA

ABSTRACT

The differential phase contrast CT (DPC-CT) implemented with x-ray tube and grating is emerging as a new technology to improve the contrast sensitivity of the conventional CT. Via system modeling, analysis and computer simulation, we investigate the DPC-CT's characteristics of signal and noise and compare them with the conventional CT. The preliminary data show that the DPC-CT possesses a modulation transfer function that is comparable with that of the conventional attenuation-based CT. However, the radical difference in the noise power spectrum between the DPC-CT ($1/|k|$ trait) and the conventional CT ($|k|$ trait) leads to the substantial difference in their spectrum of noise equivalent quanta *NEQ(k)*, which accounts for the significant advantage in DPC-CT imaging performance over the conventional CT at high spatial resolution. It is believed that the finding reported in this paper can provide insightful guidelines on the research and development of DPC-CT for preclinical and clinical applications.

Index Terms— CT, x-ray phase CT, grating, differential phase contrast CT, noise power spectrum, noise equivalent quanta, contrast-to-noise ratio

1. INTRODUCTION

The differential phase contrast CT (DPC-CT) implemented with x-ray tube and grating is emerging as a new technology to improve the contrast sensitivity of the conventional CT [1-4]. The initial exploration is relatively qualitative, in which significant improvement in the soft tissue contrast in human tissue specimen or very small animals are demonstrated [1, 2]. Recently, the investigation is becoming quantitative. The noise property of the x-ray tube and grating based DPC-CT, such as the pixel-wise gross variance and contrast-to-noise ratio, have been reported [3]. However, it has been well acknowledged that the pixel-wise quality metrics are fundamentally flawed in assessing an imaging system's performance [5, 6]. The subject contrast of soft tissue in the x-ray tube and grating based DPC-CT is intrinsically determined by its refractive interaction with the x-ray beam, while the DPC-CT's imaging performance is dependent on its transfer properties of signal and noise [7]. The signal transfer property of a DPC-CT is dependent on its modulation transfer function *MTF(k)*, while its noise property can only be thoroughly characterized by the noise power spectrum *NPS(k)* [8, 9], i.e., the variation of noise intensity as a function over spatial frequency *k*. In our recently published paper [4], we reported that there exist a radical difference in the noise power spectrum between the x-ray tube and grating based differential phase contrast CT and the conventional attenuation based CT – the *NPS(k)* of the former manifests itself with the trait $1/|k|$, whereas that of the latter with the trait $|k|$. It also has been indicated that the root cause for such a radical difference is the utilization of Hilbert filter, rather than the ramp filter, in filtered back-projection algorithms, for image reconstruction in DPC-CT.

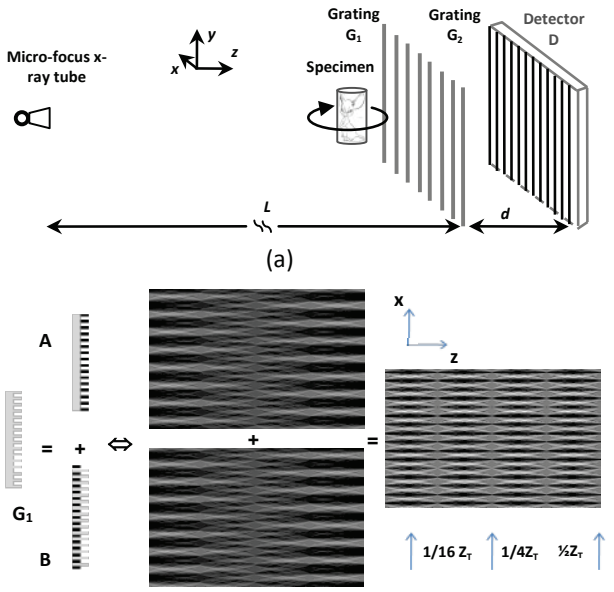


Figure 1. The schematic diagram of (a) x-ray tube and grating based DPC-CT and (b) the Talbot effect for phase retrieval.

Recognizing the important role played by the spectrum of noise equivalent quanta *NEQ(k)* in the figure of merit (FOM) to assess an imaging system's performance [5, 6], we investigate the *NEQ(k)* of the x-ray tube and grating based DPC-CT in this study. In the way analogous to what has been conducted in investigating the conventional CT's *NEQ(k)*, we treat the x-ray tube and grating based DPC-CT as a linear and shift-invariant system. Furthermore, owing to

the fact the Gaussian noise approach the Poisson photon noise if the number of photons is large, we model the noise in the x-ray tube and grating based DPC-CT system as Gaussian. Therefore, we apply the Bayesian ideal observer model to derive, analyze and evaluate the imaging performance of x-ray tube and grating based DPC-CT and compare it with that of the conventional CT, which can be utilized to predict the ultimate performance potential and identify the weak ring in the designing of the system's imaging chain.

2. CHRACTERISTICS OF SIGNAL AND NOISE

2.1. X-ray DPC-CT and its imaging mechanism

The architecture of a differential phase contrast CT implemented with a micro-focus x-ray tube and gratings [1] is shown in Fig. 1 (a). G_1 is a phase grating and G_2 an absorption grating. G_1 and G_2 work together as a shearing interferometer to detect the wavefront alteration caused by the object in the x-ray beam. A CCD x-ray detector is employed for data acquisition, in which the tube irradiates the specimen that rotates along its own axis by a range satisfying the data sufficiency condition. The key component of the imaging chain is grating G_1, a diffraction interferometer based on the Talbot effect [10]. Fig. 1 (b) shows how G_1 works by virtually decomposing it into absorption gratings *A* and *B* [4]. The extra optical path of grating *B* relative to grating *A* is half wavelength, which is equivalent to a 180° or π phase shift. The beams corresponding to gratings *A* and *B* undergo different optical paths before they reach the gratings and recombine after they pass through. Interference fringe appears if the refraction is different between the paths.

According to Fresnel analysis [11], the irradiance $I(x, z)$ at the CCD detector is

$$I_{A+B}(x,z) \cong \frac{\partial \phi(x,y)}{\partial x}\Delta x \qquad (1)$$

where Δx is a displacement in *x*-direction, and $\phi(x, y)$ is the phase corresponding to Δx, which is the projection of the refractive coeffiecient along the x-ray path *Z*

$$\phi(x,y) = \frac{2\pi}{\lambda}\int_Z \delta(x,y,z)dz\,. \qquad (2)$$

Eq. (1) shows that the irradiance depends on the derivative of the phase variation along the x-axis. After the x-ray passes G_2, the irradiance at detector *D* is [12]

$$I_{d_x,d_y}(x) = a_0(d_x,d_y) + \sum_{m=1}^{\infty} a_m(d_x,d_y)\cos\left(\frac{2\pi m x}{g_2} + \varphi_m(d_x,d_y)\right), \qquad (3)$$

where (d_x, d_y) is the coordinate in the detector and g_2 the period of grating G_2. If the object in the beam is not pure phase, i.e., it attenuates the x-ray beam, one needs to linearly shift G_2 along the x-axis. Via Fourier Analysis, one can determine $a_0(d_x, d_y)$, $a_1(d_x, d_y)$ $\varphi_1(d_x, d_y)$ from *eq*. (3). Then, one obtains

$$\frac{\partial \phi(x,y)}{\partial x} = \varphi_1(d_x,d_y)\,g_2 \Big/ \lambda z_T\,, \qquad (4)$$

where $a_0(d_x, d_y)$ and $\partial\phi(x, y)/\partial x$ are the foundation of x-ray attenuation and phase CT imaging, respectively. Substituting the $\phi(x, y)$ defined in *eq*. (2) into eq. (4), we further get

$$\varphi_1(d_x,d_y) = \frac{\lambda z_T}{g_2}\frac{\partial \phi(x,y)}{\partial x} = \frac{\lambda z_T}{g_2}\frac{\partial}{\partial x}\int_Z \delta(x,y,z)dz = \frac{\lambda z_T}{g_2}\int_Z \frac{\partial}{\partial x}\delta(x,y,z)dz \qquad (5)$$

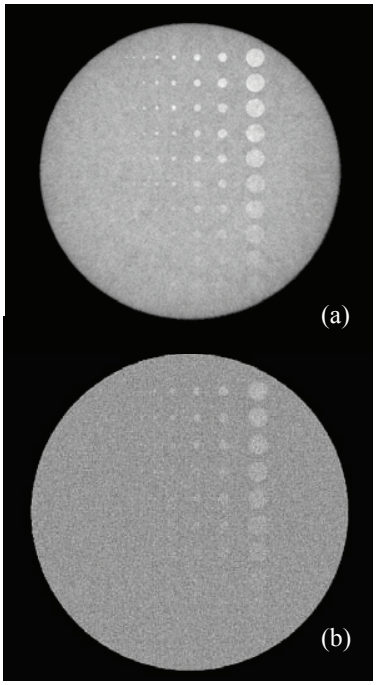


Figure 2. Transverse image of the contrast-detail phantom acquired with (a) DPC-CT and (b) conventional CT (exposure: 5×10^6 photons/cm^2·projection; detector cell: $32\times32\mu m^2$).

This means that the phase retrieved through a Fourier Analysis of *eq*. (3) is the projection of the refractive coefficient's derivative, and this is the underlying reason that the phase CT implemented with x-ray tube and gratings is called the differential phase contrast CT [1]. Once $\partial\phi(x, y)/\partial x$ and $a_0(d_x, d_y)$ are acquired, the corresponding tomographic images of attenuation and refraction can be respectively reconstructed using the filtered back-projection (FBP) algorithms [13]. Since the reconstruction of the refraction image can be carried out directly from the phase

derivative $\partial\phi(x, y)/\partial x$, the ramp kernel is replaced with the Hilbert kernel [14].

2.2. Noise equivalent quanta *NEQ(k)* of DPC-CT

The noise equivalent quanta spectrum of the conventional CT has been given as [8, 9, 15, 16]

$$NEQ_a(k) = \frac{\pi}{NPS_a(k)}|k\|MTF_a(k)|^2 \qquad (6)$$

where $NPS_a(k)$ and $MTF_a(k)$ are the noise power spectrum and modulation transfer function of the conventional CT, respectively. In parallel to eq. (6), we have derived the noise equivalent quanta of DPC-CT as

$$NEQ_p(k) = \frac{\pi}{NPS_p(k)\cdot|k|}\left|MTF_p(k)\right|^2 \qquad (7)$$

where $NPS_a(k)$ and $MTF_a(k)$ represent the noise power spectrum and modulation transfer function of the DPC-CT, respectively. Both eqs. (6) and (7) demonstrate that the noise equivalent quanta of an imaging system is jointly determined by its signal (MTF) and noise (NPS) transfer property. It should be indicated that the factor $|k|$ is on the numerator of $NEQ_a(k)$, whereas it is on the denumerator of $NEQ_p(k)$. The underlying reason account for this fundamental difference in their noise equivalent quanta is because that the $NPSa(k)$ if of the trait $|k|$, whereas the $NPS_p(k)$ possesses the trait $1/|k|$.

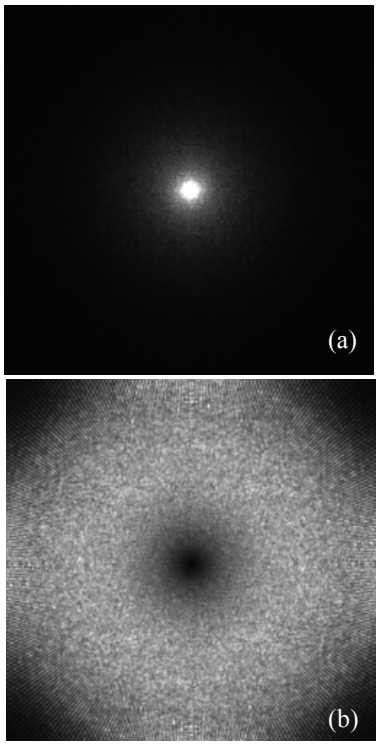


Figure 3. The noise power spectra of the (a) DPC-CT and (b) conventional CT.

3. PRELIMINARY RESULTS

Computer simulation is carried out to evaluate the imaging performance of the DPC-CT and its comparison with that of the conventional CT. The simulated x-ray exposure per projection view ranges from 10^6 to 10^9 *photon/cm*^{2} ·projection, which is comparable to that of diagnostic CT in the clinic. The x-ray photons detected by each detector cell observe Poisson distribution. The simulated detector cell size is between 32×32 μm^2 and 128×128 μm^2. Mono-chromatic x-ray source with infinitesimal focal spot at 30 *keV* is assumed in the simulation.

A cylindrical contrast-detail phantom is used to evaluate the accuracy of modeling the DPC-CT. Presented in Fig. 2 (b) is the result compared with that of the conventional CT in Fig. 1 (a). It is observed that, given the same x-ray exposure, the DPC-CT implemented with x-ray tube and grating outperform the conventional CT in the contrast-to-noise ratio at high spatial resolution. It is also observed that the noise granularity of DPC-CT is quite different from that of the conventional CT, and this is the primary reason motivating us to further investigate the signal and noise transfer property of the former.

A cylindrical water phantom is used to study the noise power spectrum of DPC-CT and its comparison with that of conventional CT. Shown in Fig. 3 (a) is the NPS of the DPC-CT, while that in Fig. 3 (b) is that of the conventional CT. It is observed that the NPS of DPC-CT is inherited with the trait of $1/|k|$, whereas that of the conventional CT with the trait $|k|$. This is a radical difference in the noise property between the DPC-CT and the conventional CT, which leads to substantial difference in their noise equivalent quanta as shown below.

A cylindrical wire phantom is used to evaluate the modulation transfer function of the DPC-CT and conventional CT, and presented in Fig. 4 are the results. It is observed that, though their imaging mechanisms are quite different, their signal transfer property characterized by the MTF are quite comparable. To assure no phase clipping occur in the DPC-CT, the wire phantom is assumed made of water placed in air. In reality, the wire made of water can be replaced with a wire of nylon or other polymers to make sure no phase clipping.

Once the noise power spectrum and modulation transfer function of the DPC CT and the conventional CT are obtained, the noise equivalent quanta of them can be readily attained using eqs. (6) and (7). Presented in Fig. 5 are the noise equivalent quanta of the DOC-CT and conventional CT, respectively. It is observed that the noise equivalent quanta of the DOC-CT and conventional CT are comparable at low spatial frequency, whereas there exists quite large difference at high spatial frequency. This means that the DPC-CT will outperform the conventional CT when the object to be imaged is small in dimension, which is desired

in practice because a lesion to be detected in the clinic is usually very small in its early stage.

4. DISCUSSIONS AND CONCLUSIONS

An investigation via computer simulation is conducted in this study to evaluate the noise equivalent quanta – the characteristics of signal (MTF) and noise (NPS) – in the DPC-CT and its comparison with that of the conventional CT. To exclude the influence of other factors on the investigation, the imaging chain of the x-ray tube and grating-based phase CT is assumed ideal. The preliminary data show that, at give detector cell size, the signal transfer property of the DPC-CT is comparable with that of the conventional CT. Consequently, owing to the fact that the NPS of the DPC-CT is of $1/|k|$ trait but that of the conventional CT of $|k|$ trait, there exist radical difference in the noise equivalent quanta of the DPC-CT and the conventional CT, as predicated by eqs. (6) and (7) and verified by the experimental result demonstrated in Fig. 5.

The research and development in the DPC-CT implemented with x-ray tube and grating has seen increasing activity recently. The results presented in this paper can provide insightful guidelines on the research and development of DPC-CT for preclinical and clinical applications. We will promptly update the community with the data obtained in our further investigation along this research direction.

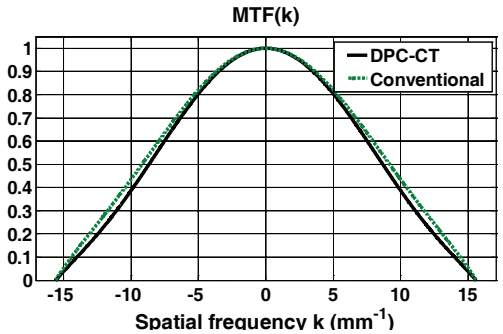


Figure 4. The modulation transfer functions of the (a) DPC-CT and (b) conventional CT (detector cell size: 32×32μm^2).

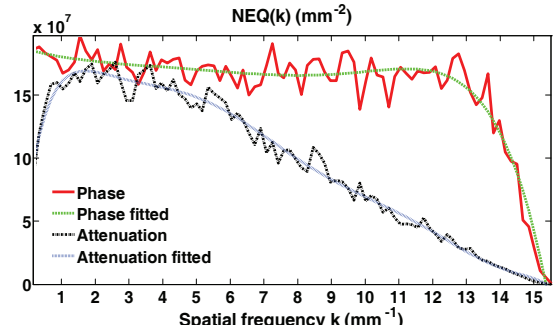


Figure 5. The noise equivalent quanta of the (a) DPC-CT and (b) conventional CT (detector cell size: 32×32 μm^2).

REFERENCES

[1] F Pfeiffer, T Weitkamp, O Bunk, C David, "Phase retrieval and differential phase-contrast imaging with low-brilliance x-ray sources," *Nature Phys.,* v.2, pp258-61, 2006.

[2] A Momose, W Yashiro, Y Takeda, Y Suzuki and T Hattori, "Phase tomography by x-ray Talbot interferometry for biological imaging," *Japan J. Applied Phys.*, v.45(6A), pp.5254-62, 2006.

[3] G Chen, J Zambelli, K Li, N Bevins and Z Qi, "Scaling law for noise variance and spatial resolution in differential phase contrast computed tomography," *Med. Phys.*, v.38, pp.584-88, 2011.

[4] X Tang, Y Yang and S Tang, "Characterization of imaging performance in differential phase contrast CT compared with the conventional CT–Noise power spectrum NPS(k)", *Med. Phys.*, v.38, pp.4386-95, 2011.

[5] H Barrett, "NEQ: its progenitors and progeny," SPIE Proc. v.7263, 72630F, 7 pages, doi: 10.1117/12.817795, 2009.

[6] CE Metz, RF Wagner, K Doi, DG Brown, RM Nishikawa and K Myers, "Toward consensus on quantitative assessment of medical imaging systems", *Med. Phys.*, v.27, pp.1057-61, 1995.

[7] JT Bushberg, JA Seibert, EM Leidholdt Jr. and JM Boone, *The Essential Physics of Medical Imaging*, 2nd ed., Philadelphia: Lippincott Williams & Wilkins, 2002.

[8] KM Hanson, "Detectability in computed tomography images," *Med. Phys.*, vol.6, pp.441-451, 1979.

[9] RF Wagner, DG Brown and MS Pastel, "Application of information theory to the assessment of computed tomography," *Med. Phys.*, v.6, pp.83-92, 1979.

[10] E Keren, O Kafri, "Diffraction effects in moiré deflectometry," *J. Opt. Soc. Am. A,* v.2, pp111-20, 1985.

[11] R Grella, "Fresnel propagation and diffraction and paraxial wave equation," *J. Optics (Paris)*, v.13, pp367-74, 1982.

[12] M Bech, TH Jensen, R Feidenhan'l, O Bunk, C David and F Pfeiffer, "Soft-tissue phase-contrast tomography with x-ray tube source," *Phys. Med. Biol.,* v.54, pp.2747-53, 2009

[13] X Tang, J Hsieh, RA Nilsen, A Hagiwara, J Thibault and E Drapkin, "A three-dimensional weighted cone beam filtered backprojection (CB-FBP) algorithm for image reconstruction in volumetric CT under a circular source trajectory," *Phys. Med. Biol.,* v.50, pp3889-905, 2005.

[14] Z Qi and G-H Chen, "Direct fan-beam reconstruction algorithm via filtered backprojection for differential phase-contrast computed tomography," *X-ray Opt. Instr.*, v.53, pp.1015-25, 2008.

[15] ICRU (International Commission on Radiation Units and Measurements), "Medical Imaging – The Assessment of Image Quality," *ICRU Report 54*, (Bethesda, MD: ICRU), pp.11-67, 1996.

[16] KL Boedeker, VN Cooper and MF McNitt-Gray, "Application of the noise power spectrum in modern diagnostic MDCT: part I. Measurement of noise power spectra and noise equivalent quanta," *Phys. Med. Biol.*, v.52, pp.4027-46, 2007.